Perturbation-free studies of single molecules

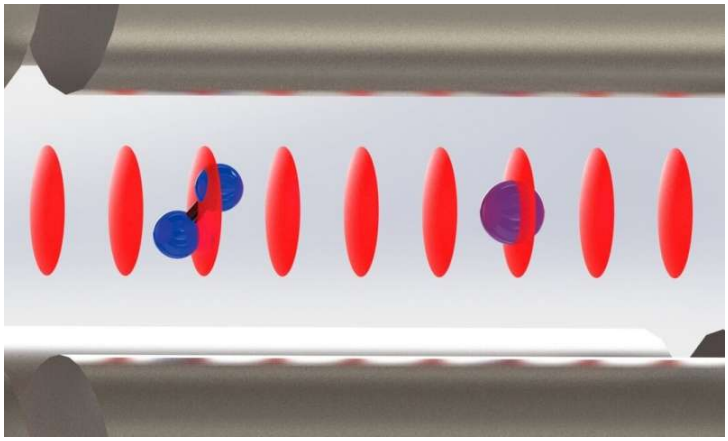

Researchers of the University of Basel have developed a new method with which individual isolated molecules can be studied precisely, without destroying the molecule or even influencing its quantum state. This highly sensitive technique for probing molecules is widely applicable and paves the way for a range of new applications in the fields of quantum science, spectroscopy and chemistry, as the journal *Science* reports.

Spectroscopic analyses are based on the interaction of matter with light and represent the most important experimental tool to study the properties of molecules. In typical spectroscopic experiments, a sample containing a large number of molecules is irradiated directly. The molecules can only absorb light at well-defined wavelengths which correspond to energy differences between two of their quantum states. This is referred to as a spectroscopic excitation.

In the course of these experiments, the molecules are perturbed and change their quantum state. In many cases, the molecules even have to be destroyed to detect the spectroscopic excitations. The analysis of the wavelengths and the intensities of these excitations provide information on the chemical structure of the molecules and their motions such as rotations or vibrations.

Inspired by quantum methods developed for the manipulation of atoms, the research group of Prof. Stefan Willitsch at the Department of Chemistry of the University of Basel has developed a new technique which enables spectroscopic measurements on the level of a single molecule, here as an example a single, charged nitrogen molecule. The new technique does not disturb the molecule or even perturb its quantum state.

In their experiments, the molecule is trapped in a radiofrequency trap and cooled down to near the absolute zero point of the temperature scale (approx. -273 °C). To enable cooling, an auxiliary atom (here a single, charged calcium atom) is simultaneously trapped and localized next to the molecule. This spatial proximity is also essential for the subsequent spectroscopic study of the molecule.

Subsequently, a force is generated on the molecule by focusing two laser beams on the particles to form a so-called optical lattice. The strength of this optical force increases with the proximity of the irradiated wavelength to a spectroscopic excitation in the molecule resulting in a vibration of the molecule within the trap instead of its excitation.

The strength of the vibration is thus related to the proximity to a spectroscopic transition and is transmitted to the neighboring calcium atom from which it is detected with high sensitivity. In this way, the same information on the molecule can be retrieved as in a conventional spectroscopic experiment.

This method, which is a new type of force spectroscopy, introduces several new concepts: First, it relies on single molecules instead of large ensembles. Second, it represents a completely non-invasive technique as detection is accomplished indirectly (via a neighboring atom) and without a direct excitation of spectroscopic transitions. Therefore, the quantum state of the molecule is left intact, so that the measurement can be repeated continuously. As a result, the method is much more sensitive than established spectroscopic methods that rely on the direct excitation and destruction of a large number of molecules.

RESEARCH ARTICLE

SPECTROSCOPY

Quantum-nondemolition state detection and spectroscopy of single trapped molecules

Mudit Sinhal*, Ziv Meir*, Kaveh Najafian, Gregor Hegi†, Stefan Willitsch‡

Trapped atoms and ions, which are among the best-controlled quantum systems, find widespread applications in quantum science. For molecules, a similar degree of control is currently lacking owing to their complex energy-level structure. Quantum-logic protocols in which atomic ions serve as probes for molecular ions are a promising route for achieving this level of control, especially for homonuclear species that decouple from blackbody radiation. Here, a quantum-nondemolition protocol on single trapped N_2^+ molecules is demonstrated. The spin-rovibronic state of the molecule is detected with >99% fidelity, and a spectroscopic transition is measured without destroying the quantum state. This method lays the foundations for new approaches to molecular spectroscopy, state-to-state chemistry, and the implementation of molecular qubits.

The impressive advances achieved in the control of ultracold trapped atoms and ions on the quantum level are now increasingly being transferred to molecular systems. Cold, trapped molecules have been created by, for example, binding ultracold atoms via Feshbach resonances (*1*) and photoassociation (*2*, *3*), molecular-beam slowing (*4*), direct laser cooling (*5*, *6*), and sympathetic cooling (*7*, *8*). The trapping of cold molecules enables experiments with long interaction times and thus paves the way for new applications, such as studies of ultracold chemistry (*9*) and precision spectroscopic measurements, which aim at a precise determination of fundamental physical constants (*10*) and their possible time variation (*11*, *12*), as well as tests of fundamental theories that reach beyond the standard model (*13*, *14*).

The complex energy-level structure and the absence of optical cycling transitions in most molecular systems constitute a major challenge for their state preparation, laser cooling, state detection, and coherent manipulation. Molecular ions which are confined in radiofrequency traps and sympathetically cooled by simultaneously trapped atomic ions (*7*, *8*) have proven a promising route for overcoming these obstacles. Recently, their rotational cooling and state preparation have been achieved (*15*–*18*), precision measurements of quantum electrodynamics and fundamental constants have been performed (*10*, *19*), the first studies of dipole-forbidden spectroscopic transitions in the mid-infrared (mid-IR) spectral domain have been reported (*20*), and state- and energy-controlled collisions with cold atoms have been realized (*21*, *22*). However, to reach, for a single molecule, the same exquisite level of control on the quantum level that can be achieved with trapped atoms (*23*), new methodological developments are required. The most promising route for achieving ultimate quantum control of molecular ions in trap experiments is offered by quantum-logic protocols (*24*), in which a co-trapped atomic ion acts as a probe for the quantum state of a single molecular ion (*25*–*27*).

Here, a quantum-logic–based quantum-nondemolition (QND) (*28*–*30*) detection of the spin-rotational-vibrational state of a single molecular nitrogen ion co-trapped with a single atomic calcium ion is demonstrated. N_2^+ is a homonuclear diatomic molecule with no permanent dipole moment, rendering all rotational-vibrational (rovibrational) transitions dipole-forbidden in its electronic ground state (*20*). Therefore, N_2^+ is an ideal test bed for precision spectroscopic studies (*31*), for tests of fundamental physics (*32*), for the realization of mid-IR frequency standards and clocks (*33*), and for implementation of molecular qubits for quantum information and computation applications (*34*, *35*).

The state-detection protocol implemented in this study relies on coherent motional excitation of the Ca^+-N_2^+ two-ion string (*36*–*38*) using an optical dipole force (ODF), which depends on the molecular state and arises from off-resonant dispersive molecule–light interactions. The excited motion was read out on the Ca^+ ion, thus preserving the state of the N_2^+ ion. State-detection fidelities >99% for the ground rovibrational state of N_2^+ were demonstrated, limited only by the chosen bandwidth of the detection cycle. Because the lifetime of the rovibrational levels in N_2^+ is estimated to be on the order of half a year (*20*), the prospects for reaching, and potentially exceeding, the high readout fidelities that are currently achieved with atomic ions (*23*, *39*) are excellent.

The present scheme has immediate applications for marked improvements of the sensitivity and, therefore, precision of spectroscopic measurements on molecular ions. This was demonstrated here by introducing a type of force spectroscopy (*40*) used to study a rovibronic component of the electronic spectrum of a single N_2^+ molecule with a signal-to-noise ratio greatly exceeding that of previous destructive detection schemes for trapped particles. Transition properties such as the line center and the Einstein A coefficient were determined and validated against the results of previous studies, which used conventional spectroscopic methods (*41*–*46*).

Quantum-nondemolition state detection

Our scheme is illustrated in Fig. 1. A detailed description of our experimental apparatus can be found in (*36*). Our setup consists of a molecular-beam machine coupled to a radiofrequency ion trap (Fig. 1A). The experiment started with loading of a small Coulomb crystal of roughly 10 $^{40}Ca^+$ ions into the trap. The atomic ions were Doppler cooled to millikelvin temperatures by scattering photons on the $(4s)^2S_{1/2} \leftrightarrow (4p)^2P_{1/2} \leftrightarrow (3d)^2D_{3/2}$ closed optical cycling transitions (Fig. 1C). A single $^{14}N_2^+$ molecular ion was then loaded into the trap using state-selective resonance-enhanced multiphoton ionization (REMPI) from a pulsed molecular beam of neutral $^{14}N_2$ molecules (*17*, *47*). This ionization scheme preferentially created N_2^+ ions in the ground electronic, vibrational and spin-rotational state, $|X^2\Sigma_g^+, v=0, N=0, J=1/2\rangle$, henceforth referred to as $|\downarrow\rangle_{N_2}$ (Fig. 1D). Here, v denotes the vibrational, N the rotational, and J the total-angular-momentum quantum numbers of the molecule, excluding nuclear spin. The ionized molecule was sympathetically cooled by the Coulomb crystal of atomic ions (*8*) within a few seconds. Then, by lowering the trap depth, Ca^+ ions were successively ejected from the trap while the molecular ion was retained in the trap, until a Ca^+-N_2^+ two-ion crystal was obtained (Fig. 1A, inset) (*36*).

The experimental sequence to detect the spin-rovibrational state of the N_2^+ ion is illustrated in Fig. 1E. First, the in-phase (*48*) motional mode of the Ca^+-N_2^+ crystal (which corresponds to the center-of-mass mode for two ions of the same mass) was cooled to the ground state of the trap, $|0\rangle$, by resolved-sideband cooling ("GSC" in Fig. 1E) on the atomic ion (*36*). The out-of-phase and the radial motional modes were maintained at Doppler-cooling temperature. At the end of the cooling cycle, the Ca^+ ion was optically pumped into its $|S_{1/2}, m=-1/2\rangle$ state, henceforth

Department of Chemistry, University of Basel, Klingelbergstrasse 80, 4056 Basel, Switzerland.
*These authors contributed equally to this work.
†Present address: RUAG Schweiz AG, Allmendstrasse 86, 3602 Thun, Switzerland.
‡Corresponding author. Email: stefan.willitsch@unibas.ch

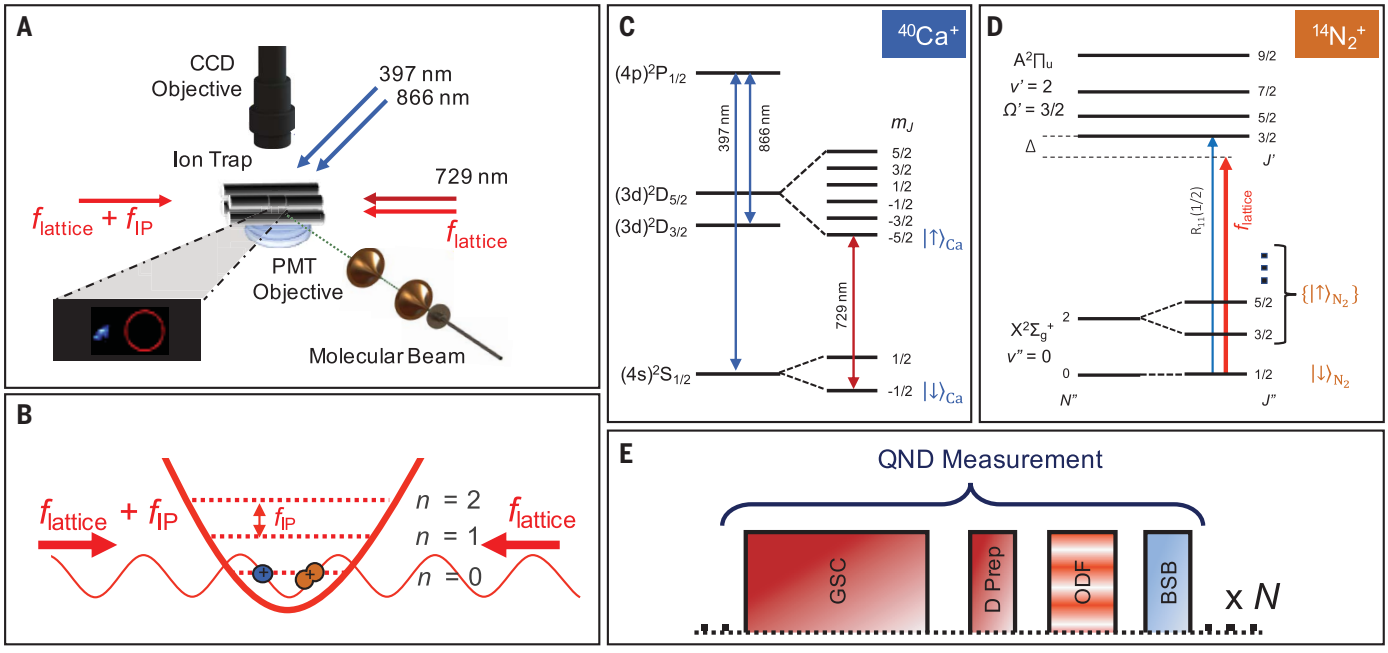

Fig. 1. Experimental scheme. (**A**) Schematic representation of the experimental setup depicting the ion trap and the molecular-beam source. The fluorescence of the atomic ion (inset) was collected by a charge-coupled device (CCD) camera. The red circle marks the position of the nonfluorescing N_2^+ molecular ion in the two-ion crystal. PMT, photomultiplier tube. (**B**) Illustration of a Ca^+-N_2^+ two-ion crystal with its in-phase external motion cooled to the ground state of the ion trap ($n = 0$), which was overlapped with two counter-propagating laser beams forming a running one-dimensional optical lattice. (**C**) Reduced energy-level diagram of $^{40}Ca^+$. The $(4s)^2S_{1/2} \leftrightarrow (4p)^2P_{1/2} \leftrightarrow (3d)^2D_{3/2}$ closed-cycling transitions (blue arrows) were used for Doppler laser cooling and for detection of the states $|\downarrow\rangle_{Ca}$ and $|\uparrow\rangle_{Ca}$. These states were coherently coupled by a narrow-linewidth laser beam (red arrow). (**D**) Reduced energy-level diagram of $^{14}N_2^+$. The lattice laser frequency, $f_{lattice}$ (red arrow), was detuned by Δ from the $R_{11}(1/2)$ transition (blue arrow). The state $|\downarrow\rangle_{N_2}$ was strongly coupled to the lattice, while all other states $\{|\uparrow\rangle_{N_2}\}$ were far detuned and hence did not couple. (**E**) Experimental sequence of a single quantum-nondemolition measurement to be repeated multiple (N) times to increase the fidelity of the determination of the molecular state. See text for details.

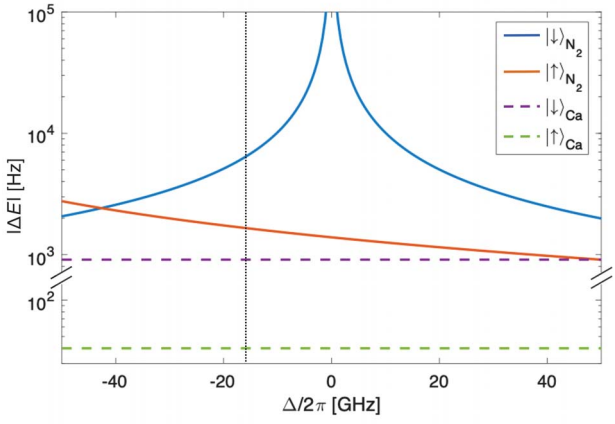

Fig. 2. Ac-Stark shift generated on N_2^+ by the one-dimensional optical lattice. Calculated magnitude of the ac-Stark shift, $|\Delta E|$, experienced by N_2^+, as a function of the laser-frequency detuning, Δ, from the $A^2\Pi_u(v' = 2) \leftarrow X^2\Sigma_g^+ (v'' = 0)$, $R_{11}(1/2)$, spin-rovibronic transition (*52*) at ~787.47 nm (*41*) for a single lattice beam of intensity 2×10^6 W/m^2. The ac-Stark shift experienced by N_2^+ when in the $|\downarrow\rangle_{N_2}$ (not in the $|\downarrow\rangle_{N_2}$) state is given by the blue (red) trace. Ca^+ in the $|\uparrow\rangle_{Ca}(|\downarrow\rangle_{Ca})$ state experienced an ac-Stark shift of 40 Hz (910 Hz) indicated by the dashed green (purple) line. The black dotted line indicates the frequency detuning, $\Delta/2\pi \approx -17$ GHz, of the optical lattice used to generate the optical dipole force, which was used for collecting the data shown in Fig. 3.

referred to as $|\downarrow\rangle_{Ca}$, where m denotes the magnetic quantum number. The Ca^+ ion was then shelved in the metastable $|D_{5/2}, m = -5/2\rangle$ state, henceforth referred to as $|\uparrow\rangle_{Ca}$, using a π-pulse on the narrow $|\uparrow\rangle_{Ca} \leftarrow |\downarrow\rangle_{Ca}$ electric-quadruple transition followed by a D-state purification pulse (*26*) ("D Prep" in Fig. 1E). This pulse allowed us to exclude experiments in which the ion was not successfully shelved to the $|\uparrow\rangle_{Ca}$ state (*49*). Preparing the Ca^+ ion in the $|\uparrow\rangle_{Ca}$ state suppressed the background signal during the state detection and thus enabled an efficient determination of the state of N_2^+ (*36*, *49*) (Fig. 2). For an ideal state preparation, the complete state of the two ions in the trap was given by $|\downarrow\rangle_{N_2}|\uparrow\rangle_{Ca}|0\rangle$.

The detection sequence was continued by applying a state-dependent ODF to excite coherent motion (*36*, *50*), the amplitude of which depends on the rovibrational state of the molecular ion ("ODF" in Fig. 1E). If the molecular ion was in the $|\downarrow\rangle_{N_2}$ state, a coherent motion of amplitude $|\alpha\rangle$ would be excited such that the probability to populate a motional Fock state, $|n\rangle$, is given by $P(n|\alpha) = |\langle n|\alpha\rangle|^2 = e^{-|\alpha|^2}|\alpha|^{2n}n!$ (*51*). If the molecular ion was in any other rotational or vibrational state, henceforth referred to as $\{|\uparrow\rangle_{N_2}\}$, a motional state $\{|\beta\rangle\}$ would be excited, where $\{|\beta|\} \ll \{|\alpha|$. Here, the curly brackets are a reminder that $\{|\uparrow\rangle_{N_2}\}$ refers to many states, all of which result in vanishingly small amplitudes of the motion, $\{|\beta|\} \ll 1$. Owing to possible experimental imperfections and decoherence—e.g., from coupling of the in-phase mode to the out-of-phase and radial modes, breakdown of the Lamb-Dicke regime because of the finite size of the lattice modulation with respect to the extent of the ion wavefunction at large excitation, imperfect ground-state cooling of the in-phase mode, or possible imperfections in the relative phase stability of the lattice beams—the underlying motional Fock-state distribution, in reality, deviated from the distribution of a perfect coherent state (*49*). However, the knowledge of

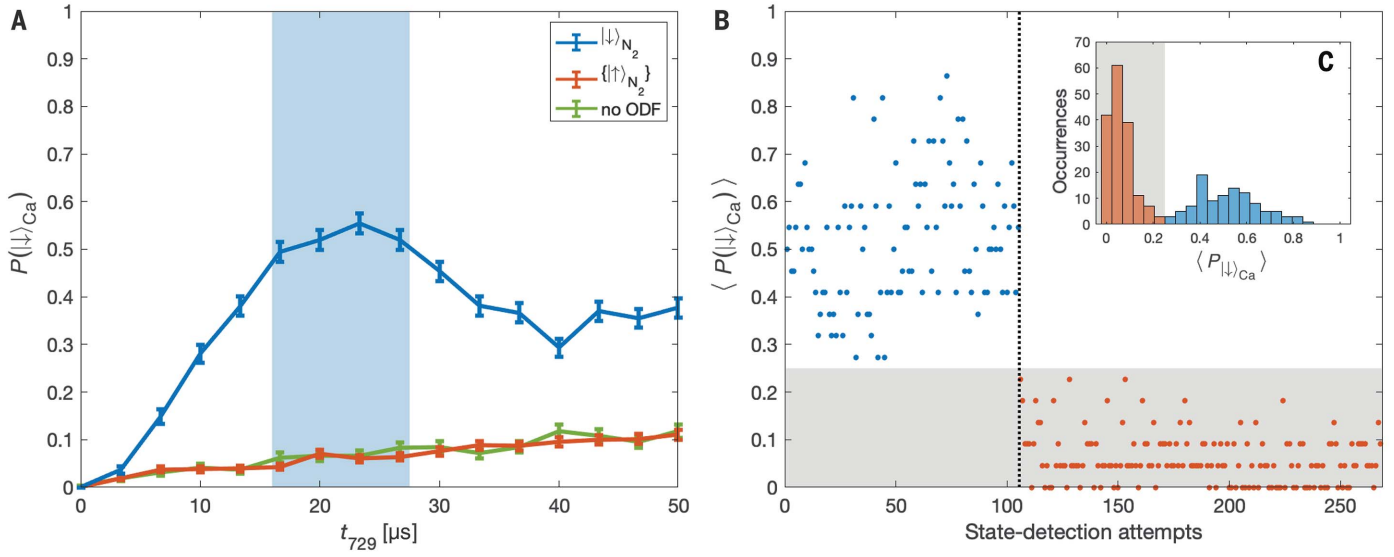

Fig. 3. Quantum-nondemolition state detection of N_2^+. (**A**) Blue-sideband (BSB) Rabi oscillation signal for N_2^+ in the $|\downarrow\rangle_{N_2}$ state (blue) and in one of the $\{|\uparrow\rangle_{N_2}\}$ states (red) as a function of the BSB pulse length t_{729}. Error bars correspond to 1σ binomial errors. The green trace represents a background measurement of the Rabi oscillation signal without ODF beams. The light-blue shaded area indicates the region of BSB pulse lengths for which maximum state-detection contrast was achieved. (**B**) Time trace of state-detection attempts. A single state-detection data point is composed of an average of 22 consecutive BSB-measurement results for pulse lengths indicated by the light-blue shaded area in (A). A threshold of $P(|\downarrow\rangle_{Ca}) = 0.25$ was used to distinguish between N_2^+ in the $|\downarrow\rangle_{N_2}$ or $\{|\uparrow\rangle_{N_2}\}$ states (gray shaded area). The blue (red) dots indicate assignment of $|\downarrow\rangle_{N_2}(\{|\uparrow\rangle_{N_2}\})$ states by the detection scheme. The dotted black line shows the onset of a quantum jump out of the $|\downarrow\rangle_{N_2}$ state to one of the $\{|\uparrow\rangle_{N_2}\}$ states. (**C**) Histogram of state-detection attempts. The gray shaded area indicates separation between $|\downarrow\rangle_{N_2}$ (blue) and $\{|\uparrow\rangle_{N_2}\}$ (red) state-detection assignments.

the exact motional state was not critical for the present molecular-state-detection protocol, as shown below.

The ODF was implemented via a state-dependent ac-Stark shift generated by two counter-propagating laser beams with frequencies $f_{lattice}$, aligned with the crystal axis, which formed a one-dimensional optical lattice (Fig. 1B). By further detuning one of the beams by the frequency of the in-phase motional mode of the two-ion crystal, $f_{IP} \approx 620$ kHz, a running optical lattice was generated, causing a modulation of the amplitude of the ac-Stark shift, which resonantly excited motion of the ion crystal depending on the rotational and vibrational state of the N_2^+ ion.

Figure 2 shows the calculated ac-Stark shift of a single lattice beam as a function of its frequency for N_2^+ in the $|\downarrow\rangle_{N_2}$ state (blue) and the maximum ac-Stark shift experienced by the N_2^+ ion when not in the $|\downarrow\rangle_{N_2}$ state (red) (*49*). The strength of the ac-Stark shift was dependent on the detuning of the lattice laser beam from spectroscopic transitions in the molecule. The peak in the ac-Stark shift of the blue trace corresponds to an on-resonance condition of the $A^2\Pi_u(v' = 2) \leftarrow X^2\Sigma_g^+(v'' = 0)$, $R_{11}(1/2)$, spin-rovibronic transition (*52*) originating from the $|\downarrow\rangle_{N_2}$ state (Fig. 1D), where $''$ ($'$) denotes the lower (upper) level of the transition. By setting the lattice-laser detuning close to this resonance, the N_2^+ ion experienced a much stronger ac-Stark shift leading to a large motional excitation $|\alpha\rangle$ when in the $|\downarrow\rangle_{N_2}$ state, as opposed to the situation where the N_2^+ ion was not in the $|\downarrow\rangle_{N_2}$ state, leading to a much weaker excitation $\{|\beta\rangle\}$. This setup ensured the state selectivity of the present scheme with respect to $|\downarrow\rangle_{N_2}$.

The state-dependent motional excitation (*36*, *37*) mapped the problem of distinguishing between the different internal states $|\downarrow\rangle_{N_2}$ and $\{|\uparrow\rangle_{N_2}\}$ of the molecule to distinguishing between different excited motional states $|\alpha\rangle$ and $\{|\beta\rangle\}$ of the two-ion crystal. The latter was achieved by Rabi sideband thermometry (*50*) on the Ca^+ ion, which shared the motional state with the N_2^+ ion. A blue-sideband (BSB) pulse using a narrow-linewidth laser at 729 nm was used to drive population between $|\uparrow\rangle_{Ca}|n\rangle \rightarrow |\downarrow\rangle_{Ca}|n-1\rangle$ states. It was followed by state-selective fluorescence on Ca^+, which projected the ion either to the $|\uparrow\rangle_{Ca}$ "dark" or the $|\downarrow\rangle_{Ca}$ "bright" state, thereby measuring the success of the BSB pulse ("BSB" in Fig. 1E). The probability of projecting to the "bright" state after the BSB pulse was approximately given by $P(|\downarrow\rangle_{Ca}) = \sum_n P(n)\sin^2(\Omega_n t_{729}/2)$ (*51*) [a more exact form is given in the supplementary materials (*49*)]. Here, t_{729} is the BSB pulse time and $\Omega_n \approx \eta\sqrt{n}\Omega_0$ is the BSB Rabi frequency, where $\eta \approx 0.1$ is the Lamb-Dicke parameter and $\Omega_0 \approx (2\pi)90$kHz is the bare Rabi frequency. The motional Fock-state population distributions were given by $P(n|\alpha)$ or $P(n|\{\beta\})$, depending on the state of N_2^+. Because $0 < P(|\downarrow\rangle_{Ca}|\{\beta\}) < P(|\downarrow\rangle_{Ca}|\alpha) < 1$, the outcome of a single BSB pulse was insufficient to determine the motional state and hence the N_2^+ internal state with high fidelity in a single shot. However, because the internal state of N_2^+ was usually not changed during the measurement, the detection sequence—i.e., cooling of the two-ion string to the motional ground state, preparing Ca^+ in the $|\uparrow\rangle_{Ca}$ state, exciting motion by the ODF, and measuring the result by a BSB pulse—could be repeated until sufficient statistics were obtained to distinguish between different molecular states. The experiment therefore represented a QND measurement (*28*–*30*). Distinguishing between the molecular states $|\downarrow\rangle_{N_2}$ and $|\uparrow\rangle_{N_2}$ is equivalent to distinguishing between two coins, α and β, with biased probabilities to get heads, *h*, in a coin toss given by $0 < p(h|\beta) < p(h|\alpha) < 1$, by repetitively flipping one of the coins *N* times. For $p(h|\alpha) = 0.52$ and $p(h|\beta) = 0.06$, a fidelity of 99.5% can be achieved in the coin (state) determination after $N = 22$ repetitive coin tosses (QND measurements) (*49*).

An experimental demonstration of the presented QND scheme for molecular-state detection is shown in Fig. 3. Here, the ODF beams were turned on for 500 μs with a single lattice-beam intensity of ~2×10^6 W/m^2. The lattice lasers were detuned by $\Delta/2\pi \approx -17$ GHz from

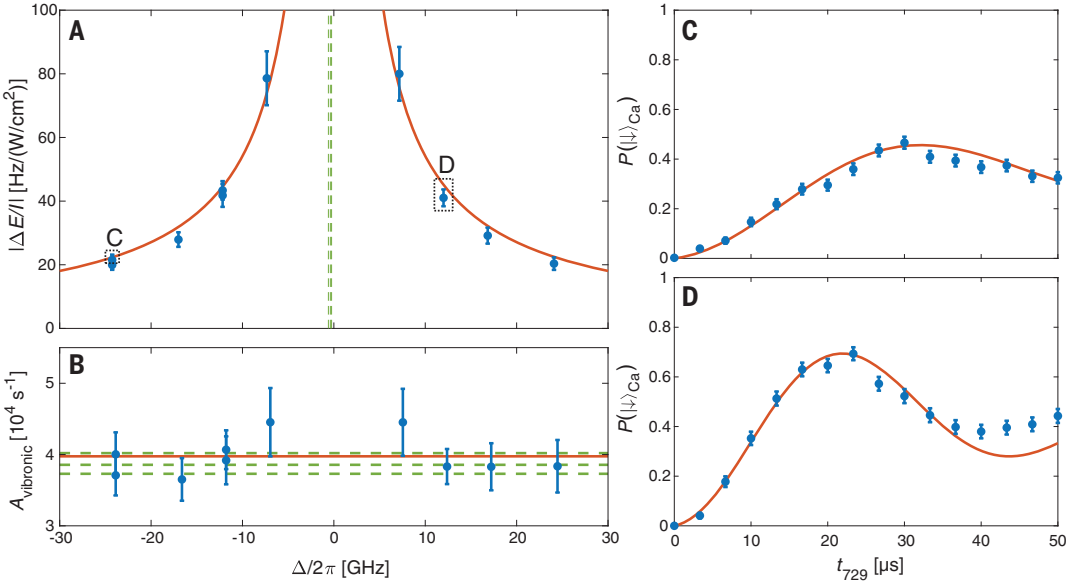

Fig. 4. Nondestructive force spectroscopy on a single N_2^+ molecule. Spectroscopic measurement of the $A^2\Pi_u(v'=2)\leftarrow X^2\Sigma_g^+(v''=0)$, $R_{11}(1/2)$, transition in N_2^+. (**A**) The blue data points represent the amplitude of the ac-Stark shift, ΔE, normalized by the lattice-laser intensity, I, and experienced by the N_2^+ ion as a function of the detuning from resonance, extracted from fits to BSB Rabi oscillation signals [(C) and (D)]. Error bars (1σ) correspond to the uncertainty in the beam intensity and in the extraction of the ODF strength from the BSB signals. The red line is a fit to the experimental data used to determine the line center. The green dashed lines indicate values of the line center reported in the literature (*41*–*43*). (**B**) The blue data points represent values for Einstein *A* coefficients of the $A^2\Pi_u(v'=2)\rightarrow X^2\Sigma_g^+(v''=0)$ vibronic transition in N_2^+ extracted from the measurements in (A). Error bars (1σ) are dominated by the measurement error of the ac-Stark shift in (A). The red line is the mean of all measurements. Different literature values (*44*–*46*) are given by the dashed green lines. (**C** and **D**) Two examples of observed BSB Rabi oscillation signals (blue) for the N_2^+ ion in the $|\downarrow\rangle_{N_2}$ state for lattice-laser detunings, $\Delta/2\pi$, of about −25 GHz and +25 GHz, respectively. Error bars (1σ) correspond to statistical binomial errors. The red line is a fit to determine the ac-Stark shift experienced by the molecule at the respective lattice-laser detunings (*49*).

the $R_{11}(1/2)$ transition (Figs. 1D and 2). The BSB pulse time, t_{729}, was scanned in order to observe Rabi oscillations, shown in Fig. 3A. When the N_2^+ ion was in the $|\downarrow\rangle_{N_2}$ state, a strong Rabi oscillation was observed (blue), in contrast to when the N_2^+ ion was in one of the $\{|\uparrow\rangle_{N_2}\}$ states, where almost no oscillation was observed (red). The residual signal of the $\{|\uparrow\rangle_{N_2}\}$ states is attributed to imperfect ground-state cooling of the two-ion crystal rather than motional excitation by the lattice beams, as can be seen from a comparison to the background signal (green) obtained when the ODF beams were completely turned off.

For the parameters used in the experiment shown in Fig. 3A, the maximum contrast between the $|\downarrow\rangle_{N_2}$ and the $\{|\uparrow\rangle_{N_2}\}$ signals was reached at $t_{729}\approx 20$ μs. For this BSB pulse time, $P(|\downarrow\rangle_{Ca}|\alpha)=0.52$ and $(P(|\downarrow\rangle_{Ca}|\{\beta\})=0.06$, such that 22 QND measurements were sufficient to distinguish between the states at a confidence level of 99.5% (*49*). A lower number of QND measurements would result in a reduced level of confidence for the state determination. Although a higher number of QND measurements would increase the detection fidelity, it would reduce the duty cycle of state determinations. This would imply a smaller number of state-determination attempts before a state-changing event, such as off-resonant photon scattering or inelastic collision with background gas molecules, occurs. Therefore, 22 was chosen as the number of QND measurements per state-detection attempt to optimize the overall fidelity. Such a QND determination of the N_2^+ state is shown in Fig. 3B. The BSB success probability, $P(|\downarrow\rangle_{Ca})$, was determined from the average of the results of 22 BSB pulses with pulse times in the range of 16.7 to 26.7 μs (light-blue shaded area in Fig. 3A). A threshold of $P(|\downarrow\rangle_{Ca})=0.25$ was set to determine whether the molecule was in the $|\downarrow\rangle_{N_2}$ ("bright" molecule) or $\{|\uparrow\rangle_{N_2}\}$ ("dark" molecule) state (blue or red dots in Fig. 3B, respectively). The molecular state was repeatably determined to be "bright" 105 times with zero false detections. Afterward, the molecular state was repeatedly determined to be "dark" 163 times with zero false detections. Using Bayesian inference, the experimentally inferred fidelity was 99.1(9)% and 99.4(6)% for the "bright" and "dark" states, respectively. The sudden change in the state of the molecule from "bright" to "dark" during the experiment was due to a quantum jump that was most likely caused by a state-changing collision with a background gas molecule in our vacuum system at a pressure of 1×10^{-10} mbar. The rate of these state-changing events, together with other types of inelastic processes, such as chemical reactions, is proportional to the partial pressure of background gas molecules in our vacuum system (N_2, H_2O, H_2, and others).

Force spectroscopy

Because the state-detection signal is proportional to the ac-Stark shift experienced by the molecule, it was used to perform measurements of spectroscopic transitions in the molecule. Such a spectroscopic experiment is demonstrated on the $R_{11}(1/2)$ spin-rotational component of the $A^2\Pi_u(v'=2)\leftarrow X^2\Sigma_g^+(v''=0)$ electronic-vibrational transition in N_2^+ (Fig. 4). Rabi oscillations on the BSB transition in Ca^+ resulting from the ODF acting on a molecule in the $|\downarrow\rangle_{N_2}$ state were measured for different detunings of the lattice-laser beams from this resonance. As the resonance was approached, the ac-Stark shift increased as ~$1/\Delta$, leading to a larger excitation, $|\alpha\rangle$, of the ion crystal. The magnitude of the ac-Stark shift was extracted from a fit to the Rabi-oscillation signal (Fig. 4, C and D). The fitting function was experimentally determined by applying a well-defined force on the Ca^+ ion when the N_2^+ ion was in one of the $\{|\uparrow\rangle_{N_2}\}$ states and experienced no force (*49*). The use of an experimentally determined fitting function circumvented the need for characterizing the exact motional state, which may deviate from ideal coherent motion (*49*). For the chosen ODF pulse length of 500 μs, the Rabi signal was sensitive to ac-Stark shifts in the interval from 2.5 to 13 kHz. To extend the dynamic range of our measurement, the lattice-beam powers were scaled to keep the Rabi signal within the experimental sensitivity range.

Figure 4A depicts such a force spectrum of this transition. The experimentally measured ac-Stark shifts were fitted with an ~$1/|f-f_0|$ ac-Stark–shift profile to determine the line center, f_0 = 380.7011(2) THz, which agrees well with previous measurements (*41*–*43*) using ensembles of molecules that yielded results in the range f_0 = 380.7007(3) THz (dashed green lines in Fig. 4A). The precision of our

measurement could be enhanced by using smaller detunings, but only at the expense of an increased probability of scattering a photon at the molecule by the lattice beams and thus losing the molecular state. As an example, for the current experimental parameters of ~10 GHz detuning and ~10 kHz ac-Stark shift, an average of 1000 high-fidelity QND state determination cycles (20,000 BSB pulses) can be expected before the molecular state is lost owing to off-resonant scattering (*49*). Decreasing the detuning to 100 MHz would reduce the number of expected QND state determinations to 10 (200 BSB pulses) owing to the $1/\Delta^2$ scaling of the scattering rate (compared with the ac-Stark shift scaling of $1/\Delta$). Nevertheless, these measurements should be possible with efficient and reliable replenishment of molecular ions in the trap. For such close detunings, our method is expected to be sensitive to the hyperfine structure of the transition (*53*), which was not resolved here and has, to our knowledge, not yet been experimentally studied. In this experiment, the absolute accuracy of the wavemeter used to evaluate the lattice-laser frequency was estimated to be better than 50 MHz by repetitive measurements of the $P_{3/2} \leftarrow D_{5/2}$ spectroscopic transition in Ca^+ during the experiment.

The electronic-vibrational (vibronic) part of the Einstein A coefficient, A_{vibronic}, of the $A^2\Pi_u(v'=2) \rightarrow X^2\Sigma_g^+(v''=0)$ transition was extracted from the ac-Stark–shift measurements as shown in Fig. 4B. For each ac-Stark–shift determination, $\Delta E(\Delta)$ (Fig. 4A), a corresponding value $A_{\mathrm{vibronic}}(\Delta)$ was calculated. The mean value of $A_{\mathrm{vibronic}} = 3.98(11) \times 10^4\ \mathrm{s}^{-1}$ is in good agreement with previous results in the range $A_{\mathrm{vibronic}} = 3.87(14) \times 10^4\ \mathrm{s}^{-1}$ (*44*–*46*) (Fig. 4B, dashed green lines). The two data points with the smallest detuning in Fig. 4B seem to slightly deviate from the other points. This effect might be due to the unresolved hyperfine structure of the transition, which becomes nonnegligible at close detunings. Nevertheless, all points were included in the determination of A_{vibronic}.

Outlook

A QND detection of the internal quantum state of a single molecule with >99% fidelity has been demonstrated. The fidelity of the state detection was not limited by the state lifetime and off-resonant scattering, as is the case in atomic ions (*23*, *39*), and hence it can be increased even further, at the expense of a slower data acquisition rate. On the basis of this detection scheme, an approach for measuring spectroscopic line positions and transition strengths in molecules using force spectroscopy has been realized.

The approach presented here can be compared to the pioneering experiment of Wolf *et al.* (*25*), in which a motional qubit was implemented to detect the internal states of polar MgH^+ molecules. Our scheme allows a simpler approach for state detection by coherently exciting motion, which also readily enables the extraction of accurate values for spectroscopic quantities such as transition strengths. Here, a set of tools was developed for the state preparation and quantum manipulation of apolar N_2^+ molecules, which do not couple to the blackbody radiation field. Although immunity to blackbody radiation imposes additional technical challenges, it makes apolar species such as N_2^+ attractive systems, as demonstrated here by the excellent state-detection fidelity.

The present QND scheme should be universally applicable to both polar and apolar molecular ions. It represents a highly sensitive method to repeatedly and nondestructively read out the quantum state of a molecule and thus introduces a molecular counterpart to the state-dependent fluorescence on closed-cycling transitions, which forms the basis of sensitive readout schemes in atomic systems (*23*, *39*). It enables state-selected and coherent experiments with single trapped molecules with duty cycles several orders of magnitude higher than previous destructive state-detection schemes (*15*, *20*). It thus lays the foundations for vast improvements in the sensitivity and, therefore, precision of spectroscopic experiments on molecular ions, as discussed in (*36*). The possibility for efficient, nondestructive state readout also lays the foundation for the application of molecular ions in quantum-information and coherent-control experiments, as are currently being performed with great success using atomic ions (*23*). In this context, the potentially long lifetimes and coherence times of molecular states may offer previously unexplored possibilities for, for example, realizing quantum memories. Additionally, the present scheme also enables studies of cold collisions and chemical reactions between ions and neutrals with state control on the single-molecule level, offering prospects for the exploration of molecular collisions and chemical reaction mechanisms in unprecedented detail. Finally, our approach could be used not only to detect the quantum state of a single molecule but also to prepare a quantum state through a projective measurement down to the Zeeman level (*36*), unlike previous schemes (*15*, *17*), which could prepare only the rovibronic level of the molecule. The present scheme thus also potentially represents a key element in the methodological toolbox of the burgeoning field of molecular quantum technologies and the realization of molecular qubits encoded in the rovibrational spectrum.

REFERENCES AND NOTES

1. K.-K. Ni *et al.*, *Science* **322**, 231–235 (2008).
2. J. M. Sage, S. Sainis, T. Bergeman, D. DeMille, *Phys. Rev. Lett.* **94**, 203001 (2005).
3. L. R. Liu *et al.*, *Science* **360**, 900–903 (2018).
4. S. Y. T. van de Meerakker, H. L. Bethlem, N. Vanhaecke, G. Meijer, *Chem. Rev.* **112**, 4828–4878 (2012).
5. J. F. Barry, D. J. McCarron, E. B. Norrgard, M. H. Steinecker, D. DeMille, *Nature* **512**, 286–289 (2014).
6. L. Anderegg *et al.*, *Nat. Phys.* **14**, 890–893 (2018).
7. K. Mølhave, M. Drewsen, *Phys. Rev. A* **62**, 011401 (2000).
8. S. Willitsch, *Int. Rev. Phys. Chem.* **31**, 175–199 (2012).
9. S. Ospelkaus *et al.*, *Science* **327**, 853–857 (2010).
10. S. Alighanbari, M. G. Hansen, V. I. Korobov, S. Schiller, *Nat. Phys.* **14**, 555–559 (2018).
11. S. Schiller, V. Korobov, *Phys. Rev. A* **71**, 032505 (2005).
12. K. Beloy *et al.*, *Phys. Rev. A* **83**, 062514 (2011).
13. M. S. Safronova *et al.*, *Rev. Mod. Phys.* **90**, 025008 (2018).
14. D. DeMille, J. M. Doyle, A. O. Sushkov, *Science* **357**, 990–994 (2017).
15. P. F. Staanum, K. Højbjerre, P. S. Skyt, A. K. Hansen, M. Drewsen, *Nat. Phys.* **6**, 271–274 (2010).
16. T. Schneider, B. Roth, H. Duncker, I. Ernsting, S. Schiller, *Nat. Phys.* **6**, 275–278 (2010).
17. X. Tong, A. H. Winney, S. Willitsch, *Phys. Rev. Lett.* **105**, 143001 (2010).
18. C.-Y. Lien *et al.*, *Nat. Commun.* **5**, 4783 (2014).
19. J. Biesheuvel *et al.*, *Nat. Commun.* **7**, 10385 (2016).
20. M. Germann, X. Tong, S. Willitsch, *Nat. Phys.* **10**, 820–824 (2014).
21. T. Sikorsky, Z. Meir, R. Ben-Shlomi, N. Akerman, R. Ozeri, *Nat. Commun.* **9**, 920 (2018).
22. A. D. Dörfler *et al.*, *Nat. Commun.* **10**, 5429 (2019).
23. T. P. Harty *et al.*, *Phys. Rev. Lett.* **113**, 220501 (2014).
24. P. O. Schmidt *et al.*, *Science* **309**, 749–752 (2005).
25. F. Wolf *et al.*, *Nature* **530**, 457–460 (2016).
26. C. W. Chou *et al.*, *Nature* **545**, 203–207 (2017).
27. C. W. Chou *et al.*, arXiv:1911.12808 [physics.atom-ph] (28 November 2019).
28. V. B. Braginsky, Y. I. Vorontsov, K. S. Thorne, *Science* **209**, 547–557 (1980).
29. V. B. Braginsky, F. Y. Khalili, *Rev. Mod. Phys.* **68**, 1–11 (1996).
30. D. B. Hume, T. Rosenband, D. J. Wineland, *Phys. Rev. Lett.* **99**, 120502 (2007).
31. M. Kajita, *Phys. Rev. A* **92**, 043423 (2015).
32. M. Kajita, G. Gopakumar, M. Abe, M. Hada, M. Keller, *Phys. Rev. A* **89**, 032509 (2014).
33. S. Schiller, D. Bakalov, V. I. Korobov, *Phys. Rev. Lett.* **113**, 023004 (2014).
34. H. J. Kimble, *Nature* **453**, 1023–1030 (2008).
35. S. Wehner, D. Elkouss, R. Hanson, *Science* **362**, eaam9288 (2018).
36. Z. Meir, G. Hegi, K. Najafian, M. Sinhal, S. Willitsch, *Faraday Discuss.* **217**, 561–583 (2019).
37. D. B. Hume *et al.*, *Phys. Rev. Lett.* **107**, 243902 (2011).
38. J. C. Koelemeij, B. Roth, S. Schiller, *Phys. Rev. A* **76**, 023413 (2007).
39. J. E. Christensen *et al.*, arXiv:1907.13331 [quant-ph] (31 July 2019).
40. M. J. Biercuk, H. Uys, J. W. Britton, A. P. VanDevender, J. J. Bollinger, *Nat. Nanotechnol.* **5**, 646–650 (2010).
41. Y.-D. Wu *et al.*, *Chin. J. Chem. Phys.* **20**, 285–290 (2007).
42. I. H. Bachir, H. Bolvin, C. Demuynck, J. Destombes, A. Zellagui, *J. Mol. Spectrosc.* **166**, 88–96 (1994).
43. K. Harada, T. Wada, T. Tanaka, *J. Mol. Spectrosc.* **163**, 436–442 (1994).
44. D. C. Cartwright, *J. Chem. Phys.* **58**, 178–185 (1973).
45. S. R. Langhoff, C. W. Bauschlicher Jr., H. Partridge, *J. Chem. Phys.* **87**, 4716–4721 (1987).
46. F. R. Gilmore, R. R. Laher, P. J. Espy, *J. Phys. Chem. Ref. Data* **21**, 1005–1107 (1992).
47. A. Gardner, T. Softley, M. Keller, *Sci. Rep.* **9**, 506 (2019).
48. G. Morigi, H. Walther, *Eur. Phys. J. D* **13**, 261–269 (2001).
49. Materials and methods are available as supplementary materials.
50. D. M. Meekhof, C. Monroe, B. E. King, W. M. Itano, D. J. Wineland, *Phys. Rev. Lett.* **76**, 1796–1799 (1996).
51. D. Leibfried, R. Blatt, C. Monroe, D. Wineland, *Rev. Mod. Phys.* **75**, 281–324 (2003).
52. G. Herzberg, *Molecular Spectra and Molecular Structure, Volume I, Spectra of Diatomic Molecules* (Krieger, 1991).
53. P. J. Bruna, F. Grein, *J. Mol. Spectrosc.* **250**, 75–85 (2008).
54. M. Sinhal, Z. Meir, K. Najafian, G. Hegi, S. Willitsch, Raw Data for "Quantum non-demolition state detection and spectroscopy of single trapped molecules," Zenodo repository (2019); https://dx.doi.org/10.5281/zenodo.3532942.

ACKNOWLEDGMENTS

We thank A. Johnson, P. Knöpfel, G. Martin, and G. Holderied for technical support. **Funding:** Funding was provided by the Swiss National Science Foundation as part of the National Centre of Competence in Research, Quantum Science and Technology (NCCR-QSIT), grant CRSII5_183579, and by the University of Basel. **Author contributions:** M.S. and Z.M. carried out the experiments and analyzed the data. K.N. and G.H. contributed to developing the experimental methodology and setup. S.W. conceived and supervised the project. All authors contributed to the writing of the manuscript. **Competing interests:** The authors declare no competing interests. **Data and materials availability:** The raw data supporting the findings of this study are available at the Zenodo repository (*54*).

SUPPLEMENTARY MATERIALS

science.sciencemag.org/content/367/6483/1213/suppl/DC1
Supplementary Text
Fig. S1
References (*55*–*62*)

25 October 2019; accepted 31 January 2020
10.1126/science.aaz9837